

Statistical Location and Rotation-Aware Beam Search for MillimeterWave Networks

Maurizio Rea, Domenico Giustiniano, Guillermo Bielsa, Danilo De Donno, Joerg Widmer

Abstract—Beam training in dynamic millimeter-wave (mm-wave) networks with mobile devices is highly challenging as devices must scan a large angular domain to maintain alignment of their directional antennas under mobility. Device rotation is particularly challenging, as a handheld device may rotate significantly over a very short period of time, causing it to lose the connection to the Access Point (AP) unless the rotation is accompanied by immediate beam realignment. We study how to maintain the link to a mm-wave AP under rotation and without any input from inertial sensors, exploiting the fact that mm-wave devices will typically be multi-band. We present a model that maps Time-of-Flight measurements to rotation and propose a method to infer the rotation speed of the mobile terminal using only measurements from sub-6 GHz WiFi. We also use the same sub-6 GHz WiFi system to reduce the angle error estimate for link establishment, exploiting the spatial geometry of the deployed APs and a statistical model that maps the user position's spatial distribution to an angle error distribution. We leverage these findings to introduce SLASH, a Statistical Location and rotation-Aware beam Search algorithm that adaptively narrows the sector search space and accelerates both link establishment and maintenance between mm-wave devices. We evaluate SLASH with experiments conducted indoors with a sub-6 GHz WiFi Time-of-Flight positioning system and a 60-GHz testbed. SLASH can increase the data rate by more than 41% for link establishment and 67% for link maintenance with respect to prior work.

I. INTRODUCTION

Exact beam alignment of the highly directional antennas of millimeter-wave (mm-wave) communication systems is necessary to achieve high data rates or even just a sufficient link margin for communication. The need for fast and efficient beam training strategies has stimulated a variety of research studies, both theoretical and experimental [1]–[10]. There was substantial progress in terms of beam training efficiency compared to the original brute force or (optionally) hierarchical training of IEEE 802.11ad, for example through compressive beam training approaches [9], [11] that only need to scan a subspace of the available antenna beams. Nevertheless, particularly dense deployments with many devices or networks with high mobility remain a challenge. In dense networks with small cell sizes, handovers occur frequently, and a device may need to beam train with potentially many APs to determine to which APs it has the best link quality. In this case, using context information such as mobile position and angular direction from the AP to the device can provide beam steering information to speed up the link establishment without the need for explicit beam training

[10], [12]. Yet, most WiFi location systems would require additional hardware such as gyroscopes to function in the common case of device rotation for maintaining the mm-wave link. Systems using angle-of-arrival information can provide relative orientation [10], [13], but require a number of WiFi antennas that are difficult or impossible to integrate on mobile devices.

Motivated by these considerations, we propose to use a sub-6 GHz WiFi Time-of-Flight (ToF) positioning system in order to extract statistical context information for reliable mm-wave link establishment and maintenance. For ToF measurements, only a single WiFi antenna is required and they can thus be computed even with mobile and small form-factor devices. New WiFi transceivers will typically be multi-band, with a sub-6 GHz WiFi chipset complementing the mm-wave interface. Given future dense deployments with smaller communication range at mm-wave frequencies, having multiple sub-6 GHz WiFi APs in communication range of a device for ranging and positioning will be common.

We propose to estimate the angle using positioning information derived from several independent multiple sub-6 GHz WiFi links, as the exploitation of the spatial geometry of the APs allows to reduce the angle estimation error. Most importantly, we build on the insight that rotation of a mobile device affects the collected ToF ranges in the frequency domain, which can be used to estimate rotation. Our system thus not only provides position but also relative rotation information, which greatly facilitates beam maintenance and helps to avoid link disruption.

Our contributions are as follows.

- We present a model to estimate the speed of rotation of a device solely based on ToF ranging measurements. We then propose a method to infer the amount of rotation to apply to the current antenna beam to avoid mm-wave link breaks (Sec. III).
- Given ToF position estimates, we analytically derive a closed-form expression of the statistical angle error that describes the angular region that is most likely to contain the dominant angles of arrival (AoAs) and departure (AoD) of the mm-wave channel (Sec. IV).
- We design SLASH, a statistical beam search strategy based on ToF ranging and positioning information collected with sub-6 GHz measurements (Sec. V). For link establishment, we use the expression of the statistical angle error to narrow down the sector search space, ex-

exploiting the relationship between the quasi-reciprocity of the mm-wave channel and the user's position to further speed up the link establishment. For link maintenance, we propose a fast strategy to maintain the mm-wave link by tracking both device rotation and distances to APs under user mobility.

- We conduct extensive studies with a 60 GHz testbed and a sub-6 GHz WiFi ranging and positioning system (Sec. VI) to validate our approach through measurements in static and mobile scenarios where the device is carried by a human. We compare SLASH both to the 802.11ad standard and prior work. Our study indicates that SLASH is very effective in increasing the data rate with respect to prior work (Sec. VII).

II. MOTIVATION

mm-wave communication supports physical data rates of several Gb/s using highly-directional phased antenna arrays [14]. Examples of technology using mm-wave are the IEEE 802.11ad standard for Wireless Local Area Networks (WLANs) in the 60 GHz band [15] and 5G cellular networks for licensed mm-wave bands [16]. The communication between AP and User Equipment (UE) in mm-wave requires:

Link Establishment: beam training is needed to find the AoD (at the transmitter) and the AoA (at the receiver) to select an antenna sector pair that allows to establish communication and maximizes the received power.¹

Link Maintenance: after beam training, environment variations and UE mobility and rotation can cause swift changes of the link quality, and continuous beam adaptation is needed to maintain a high data rate.

However, frequently performing a time-consuming beam training procedure leads to high latency and overhead, which wastes network resources and deteriorates the system performance.

A. Beam training

We take as reference the IEEE 802.11ad beam training.² The 802.11ad standard handles the beam training procedure via a Sector Level Sweep (SLS) strategy to discover the AP-UE sector pair providing the highest received signal strength (RSS). SLS comprises two phases: (i) AP SLS and (ii) UE SLS. During the AP SLS phase, the AP exhaustively switches across all the available sectors – ideally covering the entire 360° azimuth – and transmits training frames marked with sector identifiers. The UE receives those frames with a quasi-omnidirectional antenna pattern and identifies the AP sector with the highest RSS. The same process is repeated in the subsequent UE SLS phase, where the UE trains its sectors and the AP receives quasi-omnidirectionally. Once a connection is established, the link quality degradation due

¹Note that, in this paper, we interchangeably use the terms sector and beams.

²mm-wave in 5G is under standardization, with beamforming operations for both data and control planes [16], [17]

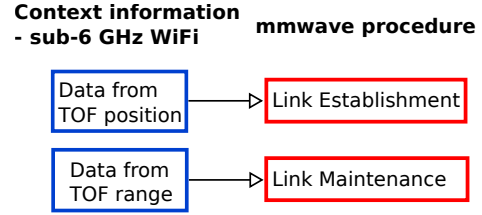


Fig. 1. Context information in SLASH for mm-wave beam search.

to user mobility is handled through either beam refinement and tracking, or through a full beam training procedure, that attempt to determine a new combination of beams with improved link quality.

B. mm-wave angle estimation with sub-6 GHz WiFi

In order to reduce the beam training delay, we investigate how well the AoD/AoA pair providing the highest RSS can be estimated by means of sub-6 GHz WiFi technology, when mm-wave and sub-6 GHz WiFi coexist in the same multi-band device.³ Previous approaches in this area are affected by two main problems.

Inferring angular rotation. First, UE rotation must be compensated for. Any variation of the angle with respect to the spatial reference system must be estimated and the chosen antenna sector adjusted accordingly, otherwise the mm-wave link quality would suffer dramatically. While additional inertial sensors such as compass and gyroscopes can be used for this purpose, they require additional hardware and continuous reading of sensor inputs. Instead, as wireless manufacturers will produce multi-band chipsets, we investigate in Sec. III how to extract rotation information from sub-6 GHz WiFi Time-of-Flight (ToF) ranges.

Errors in the angular estimation. In case of mobile devices, energy and form factor constraints limit the number of antennas to one or two, even in mobile chipsets of the last generation [10], [19]. Even if APs may be equipped with low-order MIMO transceivers in typical form factors, the median error in the angle estimation of 802.11 frames received by mobile devices with one antenna is about 20 degrees [13], [20], i.e., even in this case significant further refinement is necessary to ultimately align the antenna beams. This motivates trying alternative approaches that are less demanding in terms of hardware requirements. In our system, we use ToF position data and APs with one sub-6 GHz antenna to infer the direction of the target device. However, directly using position information to derive AoA and AoD is likely to fail, due to the typical location errors inherent in location systems. In fact, as experimentally verified later on in Sec. VII-B, just a few degrees of error in the estimation may result in a strong signal drop of the mm-wave link. We thus need a methodology that can dynamically select the set of beams where the direction of the UE/AP is statistically expected.

³The sub-6 GHz WiFi radio can also serve as a fallback in case no mm-wave link can be established [16], [18].

Based on the above observations, our approach is to design a system that uses commercial off-the-shelf sub-6 GHz WiFi devices to infer the angle information based on the distance and position estimates provided by ToF measurements. A high-level representation of the context information used in this work and how it is applied is depicted in Fig. 1.

III. FROM TOF RANGING TO ROTATION

The first challenge of our system is that, as soon as the UE rotates relative to the AP, the UE loses its antenna orientation with respect to the AP and a link maintenance procedure is required. We investigate how to address this problem using *only radio measurements* and without using any inertial sensors. In fact, we aim to avoid any application installation in the mobile UE (needed to access inertial sensors) and an increase of battery consumption caused by the inertial sensors. In addition, we cannot rely on GPS, as it is typically not available indoors, the most challenging environment for mm-wave beam search. Our insight is that a short series of ToF ranging measurements from the sub-6 GHz WiFi interfaces of the APs can provide not only the distance to compute the UE position, but also information about the relative rotation of the UE with respect to the APs. We first present the fundamental concepts for ToF ranging used in this work (see Section VI-C for further details).

A. Time-of-flight ranging

We use two-way ToF ranging for sub-6 GHz WiFi, which has the advantage of being 802.11 standard-compliant. We compute the ToF range using regular frames sent by the APs and acknowledged by the UE via 802.11 ACKs. Since the time t between each transmitted frame and ACK⁴ is deterministic, any additional delay $2 \cdot \delta_{\text{ToF}}$ can be used to infer the distance between two nodes (AP and UE nodes in our scenario). It follows that the distance d_k of sample k can be computed as $d_k = c \cdot \delta_{\text{ToF},k}$, where c is the speed of light. For a given set \mathcal{K} of samples, the client replying with ACKs adds uncertainty which can be of several clock cycles, and that can be approximated as normal distributed [21]. The effect of multipath is that the resulting distribution is the mixture of normal distributions (Gaussian Mixture Model (GMM)), with same standard deviation per distribution. Clusters are separated using iterative Expectation-Maximization (EM) algorithm on the \mathcal{K} measurements, initialized by k-means++ [22]. Finally, we take the path with the least positive mean as distance estimate \hat{d} .

B. Design of rotation estimator

Let us assume that the rotation has a central point that stays fixed, UE_0 , and a radius δ_z which represents the distance between the UE_0 and its rotation axis. Referring to Fig. 3,

⁴This is specified in the IEEE 802.11 WiFi standard as the Short Inter Frame Symbol (SIFS) duration. The real systematic time can deviate from the nominal value and can be measured experimentally.

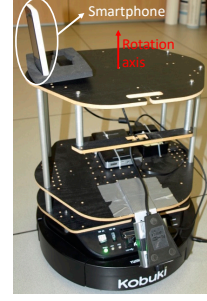


Fig. 2. The experimental setup for controlled rotation measurements.

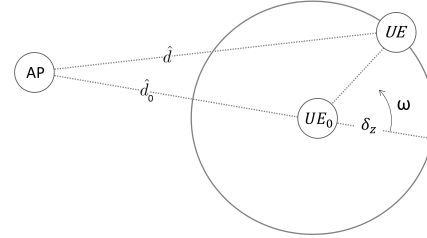


Fig. 3. Exploitation of ToF range to define the rotation speed ω .

we can define the relationship between the ToF ranging measurement \hat{d} and the rotation speed ω in polar coordinates applying the theorem of cosine as:

$$\hat{d}^2(t) = \hat{d}_0^2 + \delta_z^2 + 2\hat{d}_0\delta_z \cos(\omega t), \quad (1)$$

where $\hat{d}_0 = \|\mathbf{p}^{\text{AP}} - \hat{\mathbf{p}}^{UE_0}\|$.

From Eq. (1), a δ_z very close to zero reduces the possibility to estimate the rotation speed. However, as the mobile device is carrier by a human, in practice, δ_z is the distance between the human head and the hand (up to the arm length), and thus sufficiently bigger than zero.

Dealing with presence of multipath. In order to validate the practicality of this model when using real ToF measurements and in presence of multipath, before investigating actual human mobility, we first mount a commercial mobile phone as UE on top of a Kobuki Turtlebot II robot running ROS (Robotic Operative System), in order to produce a fixed rotation speed. The phone is located at 5 m of distance from the AP, in an open area. (The model used for the tests in this section is an Alcatel Pixi, but similar results have been achieved with other phones). A picture of the setup is shown in Fig. 2. Specifically, we consider two tests with the same UE_0 location, but with δ_z equal to 0.2 m and 0.5 m, respectively. For each experiment, we gather ToF measurements and we calculate the estimated distances using 20 samples, according to the methodology in Sec. VI. For this analysis, we make a new estimation for each collected sample, using a window that selects the last 20 samples. Next, we select only sequences of 20 samples where the number of estimated paths is one. The reason is that using sequences of samples with more than one path would cause changes to \hat{d}_0 that are not due only to the rotation.

A key aspect is how to identify the number of dominant paths (clusters) κ . Samples are distributed according to a GMM model, where each cluster identifies one Gaussian

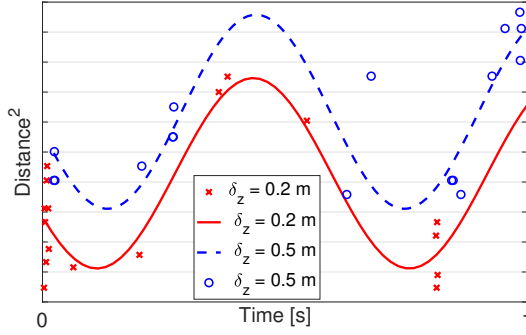


Fig. 4. Harmonic fitting of square distances in 1 s window for $\delta_z=0.2$ m and $\delta_z=0.5$ m in "ideal" case of rotation.

component. In a normal indoor environment, the number of dominant paths is typically up to 5 [23]. However, as we have a short train of packets (20 samples) and our ToF system synchronizes only to the strongest path in each sample, fewer clusters are expected and we limit the number of clusters to 3. We infer the optimal κ for the GMM statistical model selecting the model with the lowest Akaike Information Criterion (AIC) for the N measurements [24] and select only the sequences with $\kappa = 1$ for the purpose of estimating the rotation. The Fig. 4 shows the best fitted harmonic of the square distances using least squares, in a 1 s window and using the clusters with $\kappa = 1$. From the figure, we observe the amplitude differences between the two cases, due to the δ_z variations only.

Dealing with the remaining noise of the system. As the remaining multipath noise introduces high-frequency components, the result of Eq. 1 in a real case of rotation is the sum of different harmonics at different frequencies. Our analysis shows that the rotation component is located at low frequency and it becomes under transformation to the frequency domain. For this study we consider a static case both with and without rotation. In both cases, AP and UE are positioned at a distance of 5 m from each other in an open space environment where multipath can occur. For rotation, the robot on top of which the UE is mounted rotates at three speeds: 0.1, 0.35 and 0.7 rad/sec. For each experiment, we gather ranging measurements in a 1 s window, using the methodology presented above.

As samples are removed after multipath detection, we oversample the sequence to get more accurate estimates. We then interpolate the sequence, by upsampling it by a factor of ten and applying a low-pass filter. We compute the power spectral density $P(f)$, normalize it after DC removal and we introduce a criterion to estimate the rotation frequency based on the observation that faster rotations have the main harmonics at lower frequency. We integrate the normalized power spectral density and calculate $f_{1/2}$, the frequency at which the normalized power is equal to 1/2: $\sum_{f_0}^{f_{1/2}} P(f) = \frac{P_{tot}}{2}$, where f_0 is the first frequency component after the DC component and P_{tot} is the total power after DC removal. We can then estimate the rotation speed as:

$$\hat{\omega} = f_{1/2} \cdot 2\pi. \quad (2)$$

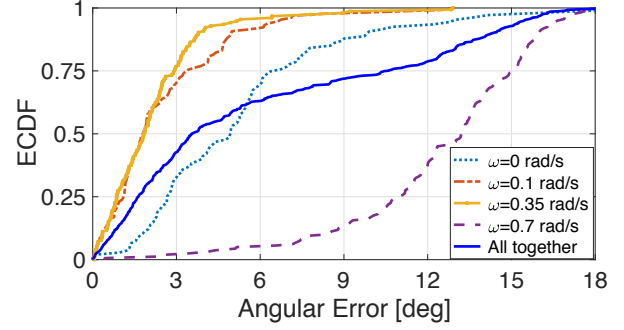


Fig. 5. ECDF of the angular error estimating the rotation speed in 1 s window.

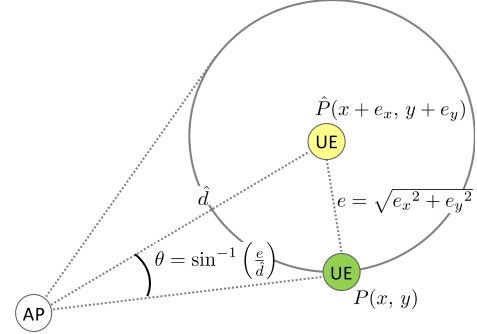


Fig. 6. Mapping user position error to angle error.

It follows that, since we analyze Eq. (1) in the frequency domain, we are able to estimate the angular speed without any knowledge of the radius δ_z , as shown in Eq. (2). We finally evaluate the accuracy of the proposed algorithm for rotation speed estimation. Fig. 5 shows the Empirical Cumulative Distribution Function (ECDF) of the rotation speed error of all cases, in degrees. Due to the noisy measurements, the proposed method has a higher angular error with very small ω , while for high ω (0.7) the method loses in accuracy due to the limited number of collected samples. Yet, as shown in the figure, we are able to estimate the rotation rate with a median error considering all scenarios of less than 4 degrees in one second (All together in the figure).

IV. ANGLE ERROR MODEL

We derive a statistical model of angle errors from the estimated location, spatial geometric information and the desired confidence level. The model will be used in the next sections to estimate where the AoD and the AoA in the mm-wave band are statistically expected, and thus accelerate the mm-wave link establishment. In our system, we consider indoor deployments with sub-6 GHz WiFi APs that can determine the UE position.

We first present the fundamental concepts for ToF positioning used in this work (see Section VI-C for further details).

A. Time-of-flight positioning

Using the distance estimates \hat{d} from at least three different APs to the UE, the UE location $\hat{\mathbf{p}}^{\text{UE}}$ is calculated

solving a non-linear least square multilateration problem via a weighted Newton-Gauss method. Weights are calculated based on the distance error of the new estimated ranges with respect to the previous computed position. The positioning system uses a time division scheduler to issue measurements rounds where only one AP at a time has the token to measure the ToF to the target device. This minimizes hidden nodes, which, based on our experience, can be frequent in a method where each AP is free to compete with other APs for accessing the medium. A final interval is allocated to drain the measurement queue of all APs. For each measurement round, the order of APs changes randomly.

B. From user position error to angle error

Let us refer to Fig. 6. We consider a scenario with a fixed AP and a mobile UE. We assume a two dimensional Cartesian coordinate system. Extension to the 3D case is straightforward. The AP position is known and equal to $\mathbf{p}^{\text{AP}} \in \mathbb{R}^{2 \times 1}$. Given $\hat{x} = x + e_x$ and $\hat{y} = y + e_y$, the UE's real and estimated positions are $\mathbf{p}^{\text{UE}} = P(x, y) \in \mathbb{R}^{2 \times 1}$ and $\hat{\mathbf{p}}^{\text{UE}} = \hat{P}(\hat{x}, \hat{y}) \in \mathbb{R}^{2 \times 1}$, respectively. The terms e_x and e_y represent the location errors on the x - and y -axis, respectively.

Let us also define $\hat{d} = \|\mathbf{p}^{\text{AP}} - \hat{\mathbf{p}}^{\text{UE}}\|$ as the estimated distance from the AP to the UE, and $e = \sqrt{e_x^2 + e_y^2}$ as the UE position error. We can then restrict the training sector space to an angular region of width 2θ , given by

$$\theta = \sin^{-1}(e/\hat{d}). \quad (3)$$

Referring to Fig. 7, the AP can avoid exhaustive beam search as in the IEEE 802.11ad standard and train only a subset of beams (namely Sectors 4, 5, and 6), which contains the sector providing maximum beamforming gain (Sector 6).

Let us define $p \in [0, 1)$ as the level of confidence of the position error. A location error e_p can be defined, which maps, in turn, to an angle error:

$$\theta_p = \sin^{-1}(e_p/\hat{d}), \quad (4)$$

which holds for $e_p \leq \hat{d}$, i.e., $\theta_p \leq \frac{\pi}{2}$ (recall that the training sector space is an angular region of width 2θ). From Eq. 4, a low p reduces the number of sectors to be trained in the beam search, but it increases the probability that the optimal sector is not included in the training. An example is shown in Fig. 7. A low $p = 0.1$ reduces the number of sectors, but it may not be sufficient to find the alignment with the highest RSS. In contrast, a larger confidence level, as such $p = 0.63$, results in a larger number of sectors, which includes the real UE position and hence the best beam.

C. Derivation of a closed-form expression

We derive a closed-form expression of the location angle error as a function of parameters that can be estimated by the positioning infrastructure and of the desired confidence

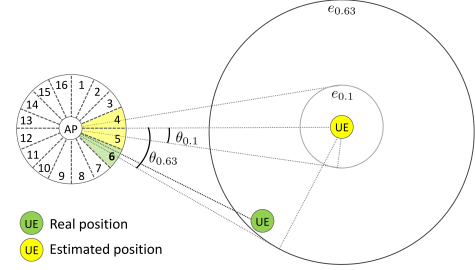


Fig. 7. Impact of the choice of two different levels of confidence for the estimated position on the location-aware beam search. As evident, choosing $\theta_{0.1}$ ($p = 0.1$) leaves out the optimal beam (green sector) from the subset of trained beams (yellow sectors).

level. Considering ranges with normal distribution (c.f. Section III-A), we can assume that the position error is a bi-variate normal distribution, where the statistical processes e_x over the x -axis and e_y over the y -axis have no correlation, and that e_x and e_y have zero mean.

We also define $\text{dRMS} = \sqrt{\sigma_x^2 + \sigma_y^2}$ as the distance root-mean-square error, where σ_x^2 and σ_y^2 are the variance of e_x and e_y , respectively. Assuming that the sources of error in the x - and y -axes have the same statistical distribution, the statistical processes e_x and e_y have identical normal distributions with $\sigma = \sigma_x = \sigma_y$. It follows that $\text{dRMS} = \sqrt{2}\sigma$. We can then resort to the error modulus $e = \sqrt{e_x^2 + e_y^2}$ to describe the position error, modeled as a Rayleigh Cumulative Distribution Function (CDF):

$$F_E(e) = \Pr(E \leq e) = 1 - e^{-\frac{e^2}{2\sigma^2}} = 1 - e^{-\frac{e^2}{\text{dRMS}^2}}. \quad (5)$$

The dRMS is often referred to as “63% error distance”, meaning that 63% of errors fall within a circle of radius dRMS, i.e., $\Pr(E \leq \text{dRMS}) \approx 0.63$ [25].

The distance error CDF in Eq. 5 can be mapped to the location angle error CDF as follows:

$$\begin{aligned} F_\Theta(\theta) &= \Pr(\Theta \leq \theta) = \Pr(\sin^{-1}(E/\hat{d}) \leq \theta) \\ &= \Pr(E \leq \hat{d} \sin \theta) = F_E(\hat{d} \sin \theta), \end{aligned} \quad (6)$$

which based on Eq. 5 can be expressed as:

$$F_\Theta(\theta) = \begin{cases} 1 - e^{-\left(\frac{\hat{d}}{\text{dRMS}} \sin \theta\right)^2} & \theta \leq \frac{\pi}{2} \\ 1 & \theta > \frac{\pi}{2}. \end{cases} \quad (7)$$

We remark that the angular error in Eq. 7 is *not* a Rayleigh function because of the trigonometric function \sin .

Computing $F_\Theta^{-1}(\theta)$, we can derive a closed-form expression of the location angle error θ_p as a function of geometric parameters and the desired confidence level $p \in [0, 1)$:

$$\theta_p = \sin^{-1} \left(\frac{\text{dRMS}}{\hat{d}} \sqrt{-\ln(1-p)} \right). \quad (8)$$

We can remove the dependence on dRMS by resorting to the Horizontal Dilution of Precision (HDOP), used in geomatics engineering to measure the multiplicative effect of the geometry of the APs on the positioning accuracy based on the (known) AP coordinates [26], [27]. The HDOP is

computed based on the *unit vector of the direction between each AP and the UE*, that is, $(\mathbf{p}_n^{\text{AP}} - \hat{\mathbf{p}}^{\text{UE}})^T / \|\mathbf{p}_n^{\text{AP}} - \hat{\mathbf{p}}^{\text{UE}}\|$. For instance, when the visible APs are in the same line as the UE or close (as it would occur measuring the distance from multiple antennas in the same AP), the geometry is unfavorable for positioning and the HDOP value is high. In contrast, in the ideal case of perfect spatial geometry (for instance APs distributed in the corners of a square), the HDOP is close to one for most of UE locations. The formal definition of the HDOP is given in the Appendix.

Using the HDOP, the dRMS can be expressed as follows [25]:

$$\text{dRMS} = \text{HDOP} \cdot \sigma_{\hat{d}}, \quad (9)$$

where $\sigma_{\hat{d}}$ is the standard deviation of the estimated distances for a specific location. Substituting Eq. 9 into Eq. 4 and computing $F_{\Theta}^{-1}(\theta)$, we can derive the following closed-form expression of the angle error θ_p :

$$\theta_p = \sin^{-1} \left(\text{HDOP} \cdot \frac{\sigma_{\hat{d}}}{\hat{d}} \sqrt{-\ln(1-p)} \right). \quad (10)$$

Estimation process. From the above analysis, the estimation process of the angle error θ_p for a given confidence value p with respect to an AP, AP_n , operates as follows:

- Estimate the UE position $\hat{\mathbf{p}}^{\text{UE}}$;
- Compute the estimated distance $\hat{d} = \|\mathbf{p}_n^{\text{AP}} - \hat{\mathbf{p}}^{\text{UE}}\|$, where $\mathbf{P}^{\text{AP}} = [\mathbf{p}_1^{\text{AP}} \ \mathbf{p}_2^{\text{AP}} \ \dots \ \mathbf{p}_N^{\text{AP}}] \in \mathbb{R}^{2 \times N}$ is the matrix containing the AP coordinates, and $\sigma_{\hat{d}}$ the standard deviation over the observation period.
- Calculate the HDOP based on \mathbf{P}^{AP} and $\hat{\mathbf{p}}^{\text{UE}}$ according to Eq. 11;
- Derive θ_p based on Eq. 10.

V. SLASH

In this section, we present SLASH, a statistical location-aware beam search strategy for mm-wave link establishment and maintenance which exploits sub-6 GHz context inputs from the ranges to the APs and from the user position. For link establishment, we assume that the LOS/quasi-LOS path is the one with the highest RSS between the AP and the UE. As shown in recent studies, when LOS/quasi-LOS is blocked, mm-wave suffers from outage and significant throughput degradation and the traffic is re-directed to sub-6 GHz WiFi [18], [28]. For link maintenance, the rotation can be estimated in presence or absence of the mm-wave LOS/quasi-LOS path.

A. Link establishment

For the link establishment, we propose a beam search algorithm to adaptively narrow the sector search space according to the statistical model of the angle error developed in Sec. IV. We assume that AP and UE employ directional sector antennas of beamwidths α_{AP} and α_{UE} , respectively, to communicate at mm-wave frequencies. We also denote p_I and p_{II} as the desired confidence levels on device position used

Phase 1: Location-aware AP SLS

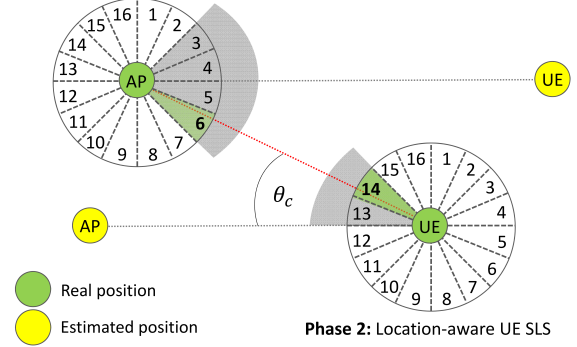


Fig. 8. Schematic representation of the working principle for link establishment.

during the AP SLS and the UE SLS phases, respectively. Starting with AP SLS as first stage, the AP can exploit the positioning system to retrieve the UE's estimated position. Then, given p_I , the location angle error θ_{p_I} is computed by the AP according to Eq. 10. The angular portion $\Theta_{p_I}^{\text{AP}} = 2\theta_{p_I}$, centered around the line joining the AP's real position and the UE's estimated position, is used to determine the subset of sectors to probe during AP SLS. As shown in the example in Fig. 8, the AP transmits training sequences to probe from beams 3 to 6, while the UE receives omnidirectionally and performs RSS measurements.

Quasi-reciprocity and position of the UE. The concept of channel quasi-reciprocity, the similarity of the downlink and uplink channels, is usually used for channel estimation [29]. We exploit it in a different way: for the UE SLS phase, we probe the sectors in the direction of the AP (as in the AP SLS phase), but given that the AP SLS already resolved the angle error at the AP side, we can take this into account to further reduce the number of sectors in the uplink to probe. For the implementation, we set $p_{II} = p_I/2$ for the UE SLS phase. For instance, considering the example in Fig. 8, the correcting effect of AP SLS allows to exclude sectors 11 and 12 from the UE SLS, leaving just two beams (13 and 14) to be probed instead of four. At the end of the two phases, the AP-UE sector pair providing the highest RSS (beams 6 and 14 in the example) is used for data transmission.

B. Link maintenance

For the link maintenance, we propose an algorithm to maintain the mm-wave communication and update the current sector using ToF measurements both for distance estimation and rotation estimation (Sec. III). As we consider static APs, UE rotations imply that only the antenna sector at the UE side needs to be updated. The key is that, while the optimal beam for the AP may not change a lot (especially if the mobile device is not very close to the AP), this is not the case with the mobile device, where each rotation can significantly impact the optimal beam.

The main algorithm steps are as follows:

- During UE mobility, as soon as the system observes a drop in signal quality, the estimated angular rotation

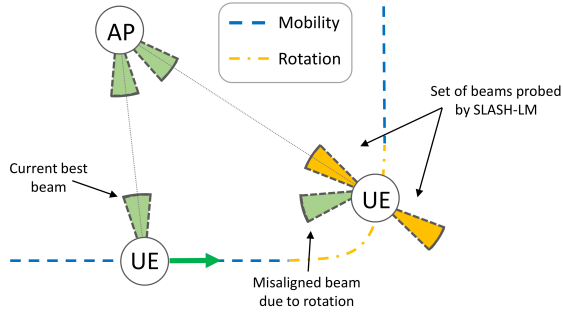


Fig. 9. Illustrative example of link maintenance using SLASH.

- since the last link establishment or maintenance is determined according to the method presented in Sec. III;
- If the angular velocity indicates a change in direction, the two candidate sectors are trained following a UE SLS-like approach (cf. Fig. 9). Note that there are a total of two candidate steering directions at the UEs for typical beamwidths, since our approach does not distinguish between clockwise and counterclockwise rotations;
 - The new direction with the highest RSS is selected for mm-wave communication. Any error in the estimated angular velocity is immediately solved using the direction with the highest mm-wave RSS as feedback loop.
 - If the angular velocity indicates no changes in direction and the mm-wave link quality is low, SLASH monitors the ToF distance estimates to the AP.
 - A beam refinement that probes the two adjacent sectors is performed when the distance estimates indicates that the UE is connected to the closest AP.
 - A handover procedure is instead triggered (with algorithm for link establishment as in Sec. V-A) when the ToF distance estimates indicate that there is a closer AP.

VI. TESTBED

Our measurements are conducted in an indoor space with an open area and offices covering a total area of 300 m². Concrete walls separate the offices from the open area, and significant multipath is present in the area. The map of the scenario is shown in Fig. 10, where red circles mark the five AP positions and green crosses mark nine randomly selected UE positions. All APs and UEs are equipped with both 60 GHz and sub-6 GHz WiFi. In our tests, AP1 and AP2 are used for mm-wave communication as they provide coverage in the open area (and the other APs do not), while all APs are used for sub-6 GHz WiFi ranging and positioning.

A. Configuration for Link Establishment

Compared to existing works in the literature which limit their investigation only to downlink transmissions [10], [12], [30], we consider both the AP SLS and UE SLS phases. An

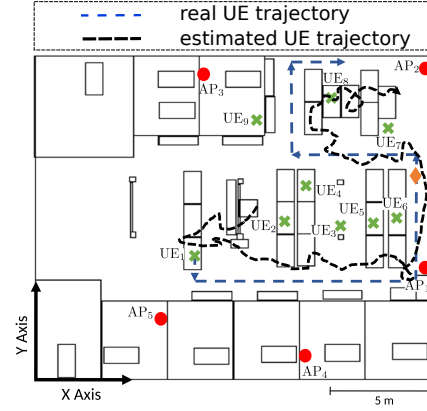


Fig. 10. Indoor environment considered for static and mobile tests.

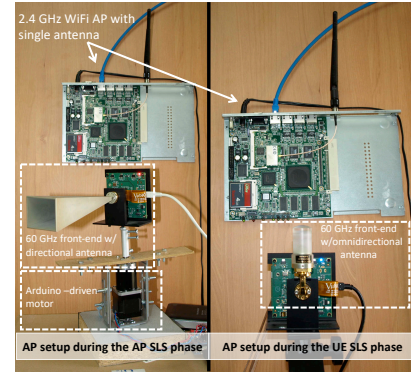


Fig. 11. 60 GHz and 2.4 GHz configuration of AP during AP SLS and UE SLS phases used for the evaluation.

illustration of the setup of the AP for these experiments is shown in Fig. 11. In order to emulate the IEEE 802.11ad AP SLS and the UE SLS link establishment phases, in our system, the mm-wave transmitter is connected to an Agilent N5182A signal generator which constantly sends a probe signal, and it is mounted on Arduino-driven stepper motors with an accuracy of 0.18 degrees in order to emulate electronically steerable phased antenna arrays. The receiver is connected to an Agilent N9010A signal analyzer to measure the RSS. In the AP SLS phase, the AP uses a Vubiq 60 GHz transmitter [31] set to 15 dBm and it is equipped with a 7°-beamwidth horn antenna. The UE uses a Vubiq 60 GHz receiver connected to an omni-directional antenna. It has a noise floor equal to −87 dBm. The opposite configuration holds in the UE SLS phase.

B. Configuration for Link Maintenance

For tests with mobility, we have to resort to simulation using a trace-driven approach since our mechanical rotation does not allow our system to operate in real-time. Other recent works in mm-wave networks have used a similar methodology [19], [32]. In this configuration, both the AP and the UE are equipped with a 7°-beamwidth antenna. Transmission power is set to 15 dBm and the noise floor is equal to −87 dBm. More specifically, we run 360/7 simu-

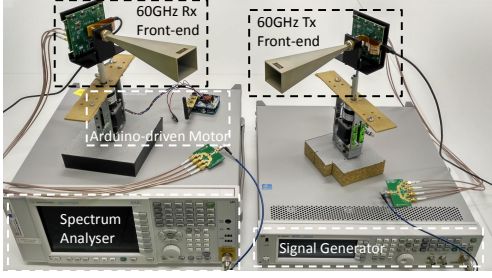


Fig. 12. The experimental setup used for 60 GHz RSS measurements once the connection has been established.

lations every step of 25 cm along the whole trajectory. We then process the output data, comparing the real human rotation speed with the estimated one using the measurement timestamps.

C. ToF positioning system

We design and build a WiFi ToF-based positioning system, where both the AP and the target use a single antenna. The ToF range is computed using regular 802.11 Probe Responses sent by the APs and acknowledged by the UE via 802.11 ACKs. We use Probe Responses rather than normal data because we experimentally observe that the UE replies only to the data packets of its associated AP, but not to those other APs. In contrast, the UE replies reliably to the Probe Responses of any AP, which is a requirement of our positioning system. In this way, ToF ranges can be computed from multiple APs to estimate the UE position. At any point in time, the target device is associated to only one AP, as in typical 802.11 wireless networks.

Our prototype positioning system uses commercial Soekris net5501 embedded machines as APs. The APs are equipped with an 802.11b/g Broadcom AirForce54G 4318 chipset operating at 2.4 GHz and one omnidirectional antenna. The Broadcom chipset runs a customized firmware and b43 driver to measure the ToF for each Probe/ACK. The APs are connected over Ethernet to the Central Location Unit (CLU) implemented in C++, that stores and processes the raw ToF data and computes the position. The CLU implements also a time-division scheduler to instruct the APs to measure the ToF ranges. The order of APs is changed after each scheduling period. The AP sends short Probe Response messages of 15 bytes of content and the target replies with an 802.11 ACK to these probes. We calculate ranges using 20 samples per AP. Tests with the mobile user have been performed by a human carrying an unmodified Alcatel Pixi smartphone.

VII. SYSTEM EVALUATION

In this section, we first experimentally validate the model introduced in Section IV, and then evaluate the performance of SLASH in static and mobile scenarios, comparing it against existing solutions in the literature.

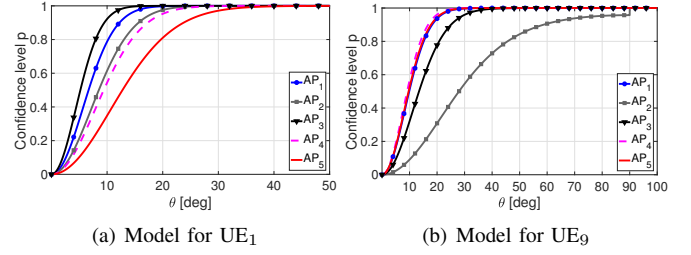


Fig. 13. Model CDF of the angle error.

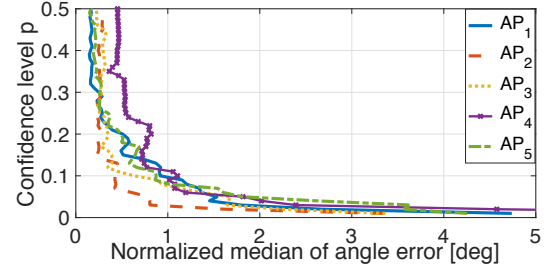


Fig. 14. Location angle error for all confidence levels: low error is observed between experimental results and theoretical outcomes.

A. Model validation

We perform extensive WiFi localization measurements in our indoor testbed shown in Fig. 10. The median positioning error of our ToF system across all (static) positions is 1.6 m. We use this data set to analyze the location angle error model introduced in Section IV. We first show in Fig. 13 the CDFs of the angle error at UE₁ and UE₉ locations using the model in Eq. 10. For the study, we use as input i) the estimated AP-UE distance \hat{d} from real experiments, ii) the standard deviation $\sigma_{\hat{d}}$ over the observation period, and iii) HDOP computed based on the known position of the five APs.

The plots in Fig. 13 confirm the dependence of the CDF on \hat{d} (c.f. Eq. 7): the larger \hat{d} , the smaller the angle θ required to achieve a desired level of confidence. The results in Fig. 13 can be used to obtain θ_p . By selecting on the y -axis a desired level of confidence p for the position estimate, we can obtain the corresponding θ_p on the x -axis.

We then assess the validity of this approach for each AP and each p , where we compare the theoretical values computed using Eq. 10 (as in Fig. 13) with the experimental distribution of θ_p . Using this data set, we then compute the median of the angle error between the experimental and the theoretical outputs across all UE positions, normalized with respect to the experimental results, and plot it in Fig. 14. We can observe that our location angle error model matches very well the experimental findings for a p level higher than 0.1. In absolute terms, our statistical model provides a median location angle error of 1.44° with $p = 0.1$ and 4.46° with $p = 0.63$ with respect to the measured one. This shows that multipath in the sub-6 GHz AP-UE links is efficiently handled by our ToF ranging and positioning system, and it does not affect significantly the validity of the model.

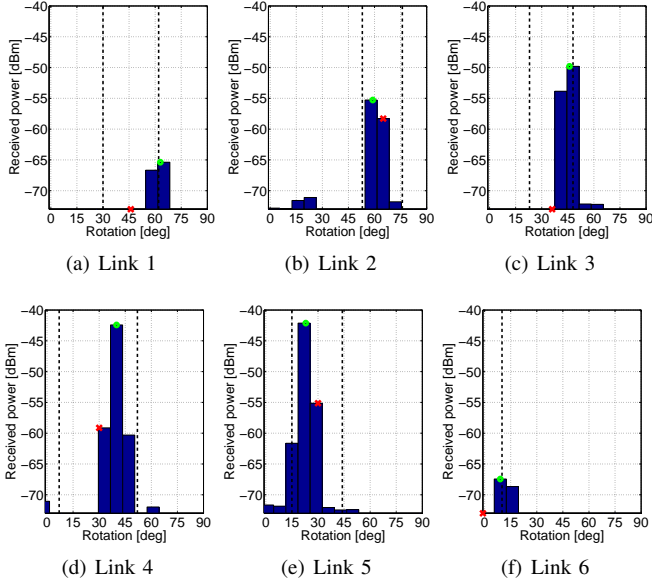


Fig. 15. Measured RSS for different directional AP-UE 60 GHz links when varying the level of misalignment between transmit and receive antennas.

B. Impact of the location error on the RSS for link establishment

We experimentally investigate how errors in the UE position estimate due to both the limited number of samples and multipath that is not resolved by the positioning system affect the 60 GHz RSS. This study is performed in a few representative positions between the UE and the AP, using directional mm-wave antennas on both nodes (cf. Fig. 12). In order to evaluate the link quality for different levels of misalignment between AP and UE antenna, we start from an ideal situation where the nodes are perfectly aligned and measure the RSS when adding different rotation drifts at steps of 7° (corresponding to the antenna beamwidth). This allows us to reproduce the effect resulting from a misaligned mm-wave link when the instantaneous output from the localization system is used to steer the devices' antenna beams.

The results are plotted in Fig. 15. The green circular markers refer to the ideal case with perfect knowledge of the AoD/AoA pair (i.e., assuming error-free sub-6 GHz location estimates). In the experiments, we only show the RSS values that are above the minimum sensitivity level required for correct frame reception. As shown in the figure, even few degrees of error in the angle estimation (red crosses) can result in steering in a direction without connectivity. The dashed black vertical lines in the figures represent the angular domain of width $2\theta_{dRMS}$, with respect to the AP position, computed applying the location angle error model in Eq. 10. From Fig. 15, we observe that, for all the links, the highest measured RSS value falls within the angular region defined by $2\theta_{dRMS}$. The validity of choosing 63% (dRMS) as a suitable confidence level results will be confirmed in the following section, applying the SLASH algorithm for link establishment to narrow down the sector search space.

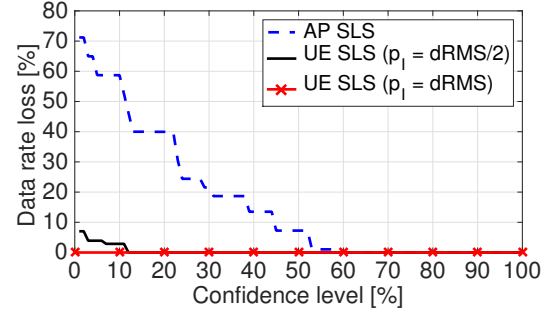


Fig. 16. Data rate loss for all possible confidence levels during the AP and UE SLS. Loss obtained comparing with respect to the standard.

C. SLASH for a static user

We consider a static user that performs the link establishment phase through the SLASH algorithm presented in Sec. V-A. We use the configuration shown in Fig. 11, and evaluate the ability of SLASH to accelerate the link establishment between AP and UE.

Data rate loss and confidence level. As a result of the successful beam search completion, the final data rate over the directional 60 GHz link established between AP and UE can be computed for the configured beams B_{best}^{AP} and B_{best}^{UE} . More specifically, the experimental RSS values and the noise floor in a 2-GHz bandwidth at 60 GHz can be translated into an achievable bit-rate R following an IEEE 802.11ad specific rate table [15]. Using these data, we study the impact of using different p_I (AP SLS phase) and p_{II} (UE SLS phase) values on SLASH performance in a total of 16 AP-UE links. Our analysis is performed feeding SLASH with the UE position estimates from the sub-6 GHz WiFi ToF positioning system. We run an exhaustive grid search, checking all the possible combinations of such parameters, and compute the data rate loss with respect to the maximum rate achievable using an exhaustive beam search instead of SLASH.

The results in Fig. 16 show that, during the AP SLS phase, setting $p_I = dRMS = 0.63$ is a reasonable choice to minimize the data rate loss. Figure 16 highlights also the benefit of exploiting the quasi-reciprocity of the mm-wave channel in SLASH as presented in Sec. V. As shown in the plot, fixing $p_I = dRMS$, the data rate loss for the UE SLS phase reaches its minimum even with the minimum confidence level. In this case we could be able to estimate the best beam just updating the steering direction. In the same figure, we also show the case $p_I = dRMS/2$, which results in a small data rate loss for small confidence levels of the UE SLS phase.

Normalized rate of SLASH for link establishment. We then compute the normalized data rate as $R \cdot \frac{T}{T+\tau}$, where R is the achieved data rate, $T=2$ ms is the data frame size, and τ is the beam search latency. In order to measure the beam search latency, we consider the typical duration of training packets according to the 802.11ad standard ($15.8 \mu s$). Fig. 17 shows the CDF of the normalized data rate for different beam search strategies. To further highlight the benefit of exploiting

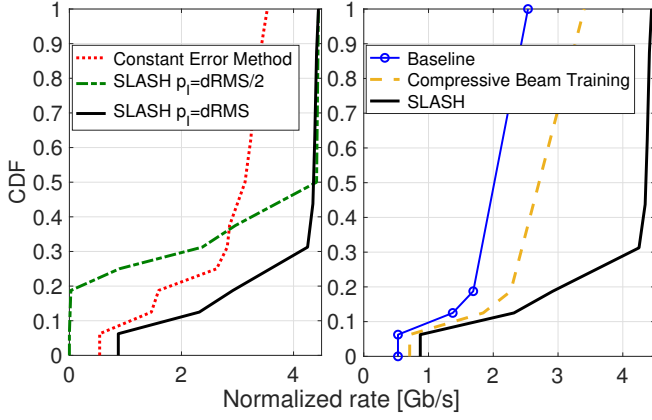


Fig. 17. ECDF of the normalized mm-wave data rate for different beam search strategies.

the quasi-reciprocity of the mm-wave channel, we show, on the left, the performance exhibited by SLASH both with $p_I = dRMS$ and $p_I = dRMS/2$, and compare it against the strategy in [30] (“Constant Error Method”) that uses a constant error for the UE position without developing any angle error model. Choosing $p_I = dRMS/2$ we can increase the average of the speed-up, at the cost of higher probability of falling back to sub-6 GHz frequencies for communication. SLASH with $p_I = dRMS$ shows the best performance, and 41% higher in median than “Constant Error Method”. We compare SLASH with $p_I = dRMS$ with other two different strategies on the right of Fig. 17, the IEEE 802.11ad as “Baseline”, and [9] (“Compressive Beam Training”). “Compressive Beam Training” adapts compressive path tracking for sector selection. SLASH achieves a data rate that is 64% higher in median than “Compressive Beam Training”. In practical cases, SLASH can achieve even higher performance than prior work, as it can exploit the knowledge of the estimated distance to APs in range to select the best moment in time for handover and performing link re-establishment phase (cf. Sec. V-B).

D. SLASH for a mobile user

We study the performance of SLASH with a user moving along the mobility pattern in Fig. 10, which includes straight-line paths and rotations. For the experimental trace, the mobile user holds the UE, walks along the trajectory at an approximated speed of 0.5 m/s and rotates at an approximated rotation speed of 0.35 rad/s. In the map in Fig. 10, we show the real trajectory of the user with the blue dashed line, while the one estimated by our positioning system is shown as black dotted line. Furthermore we use an orange diamond for the position where the user performs a handover to a second AP when the estimated ToF range indicates that it is closer to the user. For this study, we consider two APs (AP₁ and AP₂) for the user to switch between, as the other three APs are in office rooms and they could not provide good coverage along the trajectory at mmWave frequency.

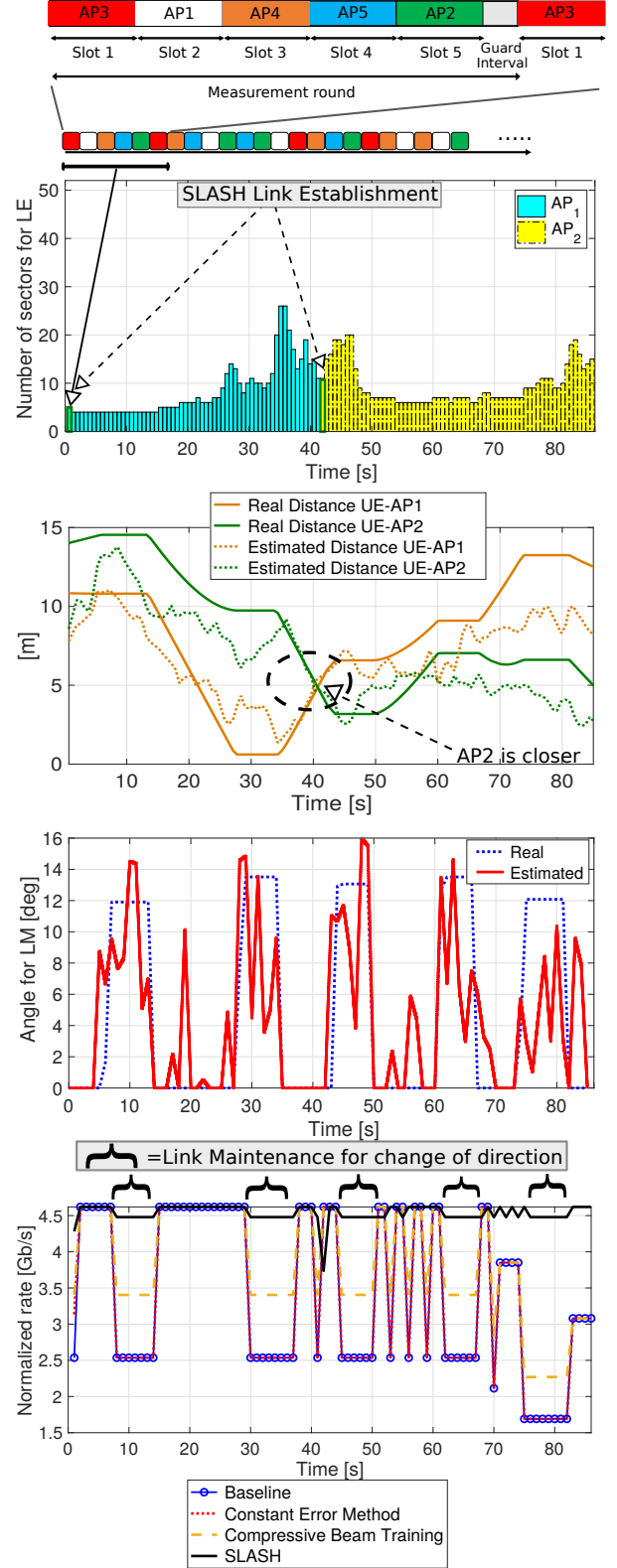


Fig. 18. Context-aware information (number of sectors for LM, angle error for LE, and distance estimate) system, and data rate of SLASH and other algorithms.

On the top of Fig. 18, we show the time division scheduler of the positioning system. Estimating the distance from each

AP, the estimated position is then available. The median error of the positioning system along the trajectory is 2.3 m. Positioning data is processed for the calculation of the angle error θ_p . The latter is used to determine the number of sectors for link establishment, based on the 7° antenna beamwidth. This results in the temporal evolution of the number of sectors shown in the second plot from the top in Fig. 18. Referring to Fig. 10, the UE is at time zero in the position UE1 marked with a green cross. Here it requests the access to the mm-wave network and the link establishment procedure of SLASH is triggered in order to establish a reliable AP-UE link. For completeness we show how many sectors would be probed over the entire trace, if the link establishment procedure would be executed at that time. After approximately 41 s, a link establishment procedure is triggered as AP_2 has better signal quality. This is performed as soon as the mm-wave link quality decreases using ToF distance estimates (third figure from the top in Fig. 18).

Using the TOF range measurements as input for the rotation estimator, we provide the angle for link maintenance. TOF range measurements are collected in each AP over the last second, and rotation estimates from different APs are integrated over the observation period. The resulting estimated rotation over time is shown in the fourth figure from the top in Fig. 18, where we have a median error of 1.54° along the whole trajectory.

We finally study the normalized data rate along the whole trajectory for four different algorithms. We recall that we resort to simulations using a trace-driven approach since our mechanical rotation does not allow our system to operate in real-time. The results are shown in the plot at the bottom in Fig. 18. SLASH tries to maintain the highest data rate, and the algorithm is called as soon as the RSS drops below the threshold for communication at the highest data rate. In addition, the user performs the handover to AP_2 according to the distance estimates of SLASH. Other strategies perform a handover as soon as the mm-wave link is below the threshold for communication. However, this does not occur in the open space under study. The plot shows the time when link maintenance is triggered due to the rotation. The "Baseline", "Constant Error Method" and "Compressive Beam Training" approaches are not able to detect rotation events and, therefore, need to resort to the same full beam search used for link establishment. During link maintenance, SLASH achieves a data rate 67% higher than "Compressive Beam Training" and 121% higher than other strategies.

VIII. RELATED WORK

The problem of fast mm-wave link establishment and maintenance is widely discussed in the literature. A comparative analysis of initial access techniques in mm-wave networks is presented in [1]. Simultaneous transmissions from multiple direction-coded beams to accelerate the beam search are exploited in [2], [3]. In [33] the authors use multi-lobe antenna patterns with random phase shifts for the beam training, which enables compressive sensing approaches to

determine AoA and AoD. This approach requires arbitrary phase shifters over the antenna elements, which is not supported by standard off-the-shelf mm-wave devices that operate with low-resolution (2-bit) RF phase shifters [34].

In [4], a link-level measurement study of indoor 60 GHz networks using a software-radio platform revealed several challenges related to human blockage and device motion and how they affect the design of MAC protocols. Some of the findings of that work have been applied to extract context information from mm-wave networks in BeamSpy [35]. BeamSpy presents a beam tracking prediction mechanism based on the channel sparsity and spatial correlation of the 60 GHz link. The proposed approach works only in static conditions, while we target mobile users. Mm-wave and sub-6 GHz WiFi context information can complement each other and can enrich the set of inputs provided for the design of MAC protocols. [9] uses compressive sensing to sweep only through a subset of probing sectors. However, the authors need still to probe a random subset of beams, while SLASH exploits knowledge from sub-6 GHz WiFi context information to probe in the direction that is statistically more likely to contain the beam with the highest RSS.

Only very few works in the literature address the problem of fast beam search in realistic, dynamic scenarios with node mobility. In [5], a protocol for mobility resilience and overhead constrained adaptation for directional 60 GHz links is presented. A "beam sounding" mechanism is introduced to estimate the link quality for selected beams, and identify and adapt to link impairments. In [36] the authors develop a zero overhead beam tracking mechanism that uses two different beam patterns during the preamble of the frames. This allows to estimate user rotation and movement. The approach does not use context information from out-of-band channels, and it requires changes in the preamble structure. In [10] an algorithm that removes in-band overhead for directional mm-wave link establishment is proposed. However, the study focuses only on static scenarios without rotation, and requires at least five antennas in both the sub-6 GHz transmitter and receiver to achieve a similar angle error as in our system.

[6] relies on gyroscope sensors to reduce the beam search under mobility. In this paper, we instead present a method that uses sub-6 GHz ToF ranges for mm-wave link maintenance. The coupling of legacy technology together with mm-wave frequencies in order to improve the beam search has been studied in some recent work. In [30], it is shown that beam training and cell discovery, respectively, can be accelerated assuming the availability of Global Positioning System (GPS) information about device locations. [30] treats the location accuracy as a given parameter without developing any angle error model based on the desired confidence level of the estimated position. Our WiFi ToF positioning system can be complemented with solutions that perform channel switching to achieve a finer-grained timing information for ranging [37] and with solutions that efficiently select the best communication technology between low frequency and mm-wave [18].

IX. CONCLUSION

In this work we investigated how context information extracted from a sub-6 GHz WiFi ToF radio ranging and positioning system can help to speed-up the beam training process in mm-wave networks. Our system did not use any inertial sensors but just radio signals. Context is extracted from a method to infer the speed of rotation of the device using ranging measurements, and from a closed-form expression of the statistical angle error model based on position and position error estimates. We then introduced SLASH, to perform statistical beam search for link establishment and maintenance, exploiting the ties between the quasi-reciprocity of the mm-wave channel and the user's position to further speed up the link establishment, and the ToF distance estimates to probe the presence of APs with better quality. We have shown through extensive experiments with a multi-band system that SLASH can significantly increase the data rate for static and mobile users compared to prior work. Our mechanism to select the number of sectors to scan based on context information can directly be integrated in multi-band WiFi devices.

APPENDIX

For the formal definition of HDOP, we denote

$$\mathbf{P}^{\text{AP}} = [\mathbf{p}_1^{\text{AP}} \quad \mathbf{p}_2^{\text{AP}} \quad \dots \quad \mathbf{p}_N^{\text{AP}}] \in \mathbb{R}^{3 \times N}$$

the matrix containing the AP coordinates. We can then define the matrix \mathbf{A} containing the unit vectors of the direction between each AP and the UE:

$$\mathbf{A} = \begin{bmatrix} (\mathbf{p}_1^{\text{AP}} - \hat{\mathbf{p}}^{\text{UE}}) / \|\mathbf{p}_1^{\text{AP}} - \hat{\mathbf{p}}^{\text{UE}}\| & -1 \\ (\mathbf{p}_2^{\text{AP}} - \hat{\mathbf{p}}^{\text{UE}}) / \|\mathbf{p}_2^{\text{AP}} - \hat{\mathbf{p}}^{\text{UE}}\| & -1 \\ \vdots & \vdots \\ (\mathbf{p}_N^{\text{AP}} - \hat{\mathbf{p}}^{\text{UE}}) / \|\mathbf{p}_N^{\text{AP}} - \hat{\mathbf{p}}^{\text{UE}}\| & -1 \end{bmatrix} \quad (11)$$

and formulate the matrix $\mathbf{Q} = (\mathbf{A}^T \mathbf{A})^{-1} \in \mathbb{R}^{4 \times 4}$. The HDOP can be then computed as:

$$\text{HDOP} = \sqrt{\mathbf{Q}_{11} + \mathbf{Q}_{22}}. \quad (12)$$

REFERENCES

- [1] M. Giordani, M. Mezzavilla, C. N. Barati, S. Rangan, and M. Zorzi, "Comparative analysis of initial access techniques in 5G mmWave cellular networks," in *2016 Annual Conference on Information Science and Systems (CISS)*, March 2016.
- [2] Y. Tsang, A. Poon, and S. Addepalli, "Coding the beams: Improving beamforming training in mmwave communication system," in *2011 IEEE Global Telecommunications Conference (GLOBECOM)*, Houston, TX, USA, Dec. 2011.
- [3] L. Chen, Y. Yang, X. Chen, and W. Wang, "Multi-stage beamforming codebook for 60GHz WPAN," in *2011 6th Int. ICST Conference on Communications and Networking in China (CHINACOM)*, Aug. 2011.
- [4] S. Sur, V. Venkateswaran, X. Zhang, and P. Ramanathan, "60 ghz indoor networking through flexible beams: A link-level profiling," in *ACM SIGMETRICS Performance Evaluation Review*, vol. 43, no. 1, 2015, pp. 71–84.
- [5] M. K. Haider and E. W. Knightly, "Mobility resilience and overhead constrained adaptation in directional 60 ghz wlans: protocol design and system implementation," in *Proceedings of the 17th ACM International Symposium on Mobile Ad Hoc Networking and Computing*. ACM, 2016, pp. 61–70.
- [6] A. Patra, L. Simić, and M. Petrova, "Experimental evaluation of a novel fast beamsteering algorithm for link re-establishment in mm-wave indoor WLANs," in *27th Annual IEEE International Symposium on Personal, Indoor and Mobile Radio Communications (PIMRC)*, Sept. 2016.
- [7] A. Alkhateeb, O. E. Ayach, G. Leus, and R. W. Heath, "Channel estimation and hybrid precoding for millimeter wave cellular systems," *IEEE Journal of Selected Topics in Signal Processing*, vol. 8, no. 5, pp. 831–846, Oct. 2014.
- [8] D. De Donno, J. Palacios, D. Giustiniano, and J. Widmer, "Hybrid analog-digital beam training for mmWave systems with low-resolution RF phase shifters," in *2016 IEEE ICC Workshop on 5G RAN Design*, May 2016.
- [9] D. Steinmetzer, D. Wegemer, M. Schulz, J. Widmer, and M. Hollick, "Compressive millimeter-wave sector selection in off-the-shelf IEEE 802.11ad devices," in *Proceedings of the 13th International Conference on Emerging Networking EXperiments and Technologies*, ser. CoNEXT '17. New York, NY, USA: ACM, 2017, pp. 414–425. [Online]. Available: <http://doi.acm.org/10.1145/3143361.3143384>
- [10] T. Nitsche, A. B. Flores, E. W. Knightly, and J. Widmer, "Steering with eyes closed: mm-wave beam steering without in-band measurement," in *2015 IEEE Conference on Computer Communications (INFOCOM)*. IEEE, 2015, pp. 2416–2424.
- [11] M. E. Rasekh, Z. Marzi, Y. Zhu, U. Madhow, and H. Zheng, "Non-coherent mmwave path tracking," in *Proceedings of the 18th International Workshop on Mobile Computing Systems and Applications*, 2017.
- [12] A. Capone, I. Filippini, and V. Sciancalepore, "Context information for fast cell discovery in mm-wave 5g networks," in *Proceedings of European Wireless 2015*. VDE, 2015, pp. 1–6.
- [13] J. Gjengset, J. Xiong, G. McPhillips, and K. Jamieson, "Phaser: Enabling phased array signal processing on commodity wifi access points," in *Proceedings of the 20th Annual International Conference on Mobile Computing and Networking*, ser. MobiCom '14. New York, NY, USA: ACM, 2014, pp. 153–164. [Online]. Available: <http://doi.acm.org/10.1145/2639108.2639139>
- [14] T. S. Rappaport, R. M. S. Sun, H. Zhao, Y. Azar, K. Wang, G. N. Wong, J. K. Schulz, M. Samimi, and F. Gutierrez, "Millimeter wave mobile communications for 5G cellular: It will work!" *IEEE Access*, vol. 1, pp. 335–349, May 2013.
- [15] IEEE standard, "IEEE 802.11ad WLAN enhancements for very high throughput in the 60 GHz band," 2012.
- [16] 3GPP, "Tr 38.802," in *Study on New Radio (NR) Access Technology - Physical Layer Aspects - Release 14*, 2017.
- [17] —, "Ts 38.811," in *NR - Physical Channels and Modulation - Release 15*, 2017.
- [18] S. Sur, I. Pefkianakis, X. Zhang, and K.-H. Kim, "Wifi-assisted 60 ghz networks," in *ACM International Conference on Mobile Computing and Networking*, ser. ACM Mobicom, 2017.
- [19] —, "Practical MU-MIMO user selection on 802.11ac commodity networks," in *Proceedings of the 22nd Annual International Conference on Mobile Computing and Networking*, ser. MobiCom '16. New York, NY, USA: ACM, 2016, pp. 122–134.
- [20] S. Sen, J. Lee, K.-H. Kim, and P. Congdon, "Avoiding multipath to revive inbuilding wifi localization," in *Proceeding of the 11th Annual International Conference on Mobile Systems, Applications, and Services*, ser. MobiSys '13. New York, NY, USA: ACM, 2013, pp. 249–262. [Online]. Available: <http://doi.acm.org/10.1145/2462456.2464463>
- [21] M. Rea, A. Fakhreddine, D. Giustiniano, and V. Lenders, "Filtering noisy 802.11 time-of-flight ranging measurements from commoditized wifi radios," *IEEE/ACM Transactions on Networking*, vol. PP, no. 99, pp. 1–14, 2017.
- [22] D. Arthur and S. Vassilvitskii, "k-means++: The advantages of careful seeding," in *Proceedings of the eighteenth annual ACM-SIAM symposium on Discrete algorithms*. Society for Industrial and Applied Mathematics, 2007, pp. 1027–1035.
- [23] M. Kotaru, K. Joshi, D. Bharadia, and S. Katti, "Spotfi: Decimeter level localization using wifi," ser. SIGCOMM '15. ACM, 2015, pp. 269–282.
- [24] S. Konishi and G. Kitagawa, *Information criteria and statistical modeling*. Springer Science & Business Media, 2008.

- [25] E. Kaplan and C. Hegarty, *Understanding GPS: principles and applications*. Artech house, 2005.
- [26] R. Langley, "Dilution of precision," *GPS World*, 1999.
- [27] C. A. Ogaja, *Geomatics Engineering: A Practical Guide to Project Design*. CRC Press, 2016.
- [28] M. Polese, M. Giordani, M. Mezzavilla, S. Rangan, and M. Zorzi, "Improved handover through dual connectivity in 5g mmwave mobile networks," *IEEE Journal on Selected Areas in Communications*, vol. 35, no. 9, pp. 2069–2084, Sept 2017.
- [29] Q. Gao, F. Qin, and S. Sun, "Utilization of channel reciprocity in advanced mimo system," in *5th International ICST Conference on Communications and Networking in China*, Aug 2010, pp. 1–5.
- [30] W. B. Abbas and M. Zorzi, "Context information based initial cell search for millimeter wave 5G cellular networks," in *2016 European Conference on Networks and Communications (EuCNC)*, June 2016, pp. 111–116.
- [31] Vubiq. V60WGD03 60 GHz Waveguide Development System. [Online]. Available: <http://www.pasternack.com/60-ghz-development-systems-category.aspx>
- [32] B. Li, Z. Zhou, W. Zou, X. Sun, and G. Du, "On the efficient beam-forming training for 60ghz wireless personal area networks," *IEEE Transactions on Wireless Communications*, vol. 12, no. 2, pp. 504–515, February 2013.
- [33] O. Abari, H. Hassanieh, M. Rodriguez, and D. Katabi, "Millimeter wave communications: From point-to-point links to agile network connections," in *Proceedings of the 15th ACM Workshop on Hot Topics in Networks*, 2016.
- [34] A. Alkhateeb, O. E. Ayach, G. Leus, and R. W. Heath, "Channel estimation and hybrid precoding for millimeter wave cellular systems," *IEEE Journal of Selected Topics in Signal Processing*, vol. 8, no. 5, pp. 831–846, Oct 2014.
- [35] S. Sur, X. Zhang, P. Ramanathan, and R. Chandra, "Beamspy: Enabling robust 60 ghz links under blockage," in *Proceedings of the 13th Usenix Conference on Networked Systems Design and Implementation*, ser. NSDI'16. Berkeley, CA, USA: USENIX Association, 2016, pp. 193–206. [Online]. Available: <http://dl.acm.org/citation.cfm?id=2930611.2930625>
- [36] A. Loch, H. Assasa, J. Palacios, J. Widmer, H. Suys, and B. Debaillie, "Zero overhead device tracking in 60 ghz wireless networks using multi-lobe beam patterns," in *Proc. ACM CoNEXT*, 2017.
- [37] J. Xiong, K. Sundaresan, and K. Jamieson, "Tonetrack: Leveraging frequency-agile radios for time-based indoor wireless localization," in *Proceedings of the 21st Annual International Conference on Mobile Computing and Networking*. ACM, 2015, pp. 537–549.